



Research Article

AOT direct and reverse micelles as a reaction media for anisotropic silver nanoparticles functionalized with folic acid as a photothermal agent on HeLa cells



Ana María Pinilla¹ · Diana Blach¹ · Stelia Carolina Mendez² · Fernando Martínez Ortega¹ 

© Springer Nature Switzerland AG 2019

Abstract

Herein, we report the synthesis of silver nanoparticles (AgNPs) using direct micelles and reverse micelles of sodium bis (2-ethylhexyl) sulfosuccinate (AOT) as reaction media. We evaluated the effect of these self-organized aggregates in the nucleation and growth mechanism of AgNPs. The results show the effect of water when it is a confined medium, where their properties are different from those of net water. These factors strongly influence the size, polydispersity and shape of nanoparticles. Moreover, the presence of ions from the reducing agents and the surfactant, it is a key factor in the anisotropy of the AgNPs obtained. For our knowledge, this is the first report in which the effect of the reaction media is evaluated by using direct and reverse micelles to synthesize silver nanoparticles. Additionally, AgNPs synthesized through the two systems were functionalized with folic acid and evaluated their cytotoxicity and photothermal properties. The results show that AgNPs synthesized through the two systems are potential photothermal agents, reaching to reduce up to 47% of the viability of the HeLa cells, using a laser of 808 nm.

Electronic supplementary material The online version of this article (<https://doi.org/10.1007/s42452-019-0894-5>) contains supplementary material, which is available to authorized users.

✉ Fernando Martínez Ortega, fmartine@uis.edu.co | ¹Centro de Investigaciones en Catálisis, Universidad Industrial de Santander, Sede Guatiguará UIS Km 2 vía Refugio, Piedecuesta, Colombia. ²Grupo de Investigación en Bioquímica y Microbiología GIBIM, Universidad Industrial de Santander, Sede Guatiguará UIS Km 2 vía Refugio, Piedecuesta, Colombia.

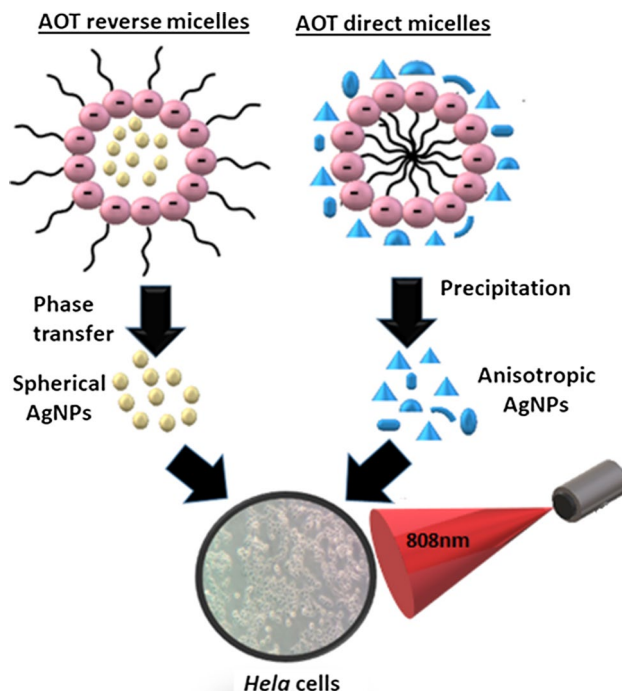


SN Applied Sciences (2019) 1:858 | <https://doi.org/10.1007/s42452-019-0894-5>

Received: 13 April 2019 / Accepted: 8 July 2019 / Published online: 15 July 2019

SN Applied Sciences
A **SPRINGER NATURE** journal

Graphic abstract



Keywords Direct micelles · Reverse micelles · Silver nanoparticles · Folic acid · Photothermal agent

1 Introduction

Metal nanoparticles (M-NPs) have been widely used in biomedical applications due to their intrinsic therapeutic properties [3, 21, 45]. In the case of silver nanoparticles (AgNPs), they have been known for their antimicrobial properties [17, 52]. However, currently it has begun to explore new applications using these such as anticancer agents [4] because they also present optical properties. These properties are associated with a phenomenon called localized surface plasmon resonance, which consisting of a collective and coherent oscillation of the free electrons of the conduction band of metallic nanoparticles [12]. This property depends on the shape and size of nanoparticles [13], and it has been used in some applications such as photothermal therapy to generate a thermal response [3, 6, 21, 36].

To prepare M-NPs, there are a great variety of methodologies [55]. One of the simple methods for synthesizing M-NPs is through the use of an excess of a strong reducing agent, for example sodium borohydride, which it has been widely used to reduce metal precursors such as silver nitrate (AgNO_3) and acid tetrachloroauric ($[\text{AuCl}_4] \cdot 3\text{H}_2\text{O}$) in aqueous medium [11, 46]. By means of this methodology, spherical nanoparticles are obtained. However,

in some applications, it is required anisotropic M-NPs (nanorods, nanotriangles, nanoprisms or nanocubes). These kinds of structures have their plasmon bands in the near infrared region (NIR), which is the most appropriate region to achieve efficiency in biological applications such as cancer photothermal therapy [22]. In The NIR region, there are two biological transparency windows located in 650–950 nm (first window) and 1000–1350 nm (second window). This region has optimal tissue transmission obtained from low scattering and energy absorption, thus providing maximum radiation penetration through tissue, without damage it [63].

In order to synthesized anisotropic M-NPs, there are many methodologies among which we should highlight: High temperature reduction method [14], electrochemical methods [54], photochemical methods [69], biosynthesis [39], and synthesis based on the use of micelles as a reaction media [60]. This last methodology has been of great interest in recent years because it is a “soft” method, in which extreme conditions of temperature and pressure are not required, besides the composition of the reaction media, allows the stability of AgNPs over time. These methodologies are based on the use of molecules with an amphiphilic character, called surfactants, which they can be solubilized in non-polar or polar medium and these

can be associated in a fluid medium to generate different types of structures such as direct and reverse micelles [15]. In direct micelles, the surfactant is oriented in such a way that the hydrophobic portion is towards inside of the micelle, leaving the hydrophilic portion in contact with the aqueous phase. In contrast, in reverse micelles, the surfactant is oriented in such a way that the hydrophilic portion is towards inside of the micelle and the hydrophobic portion is towards outside of these.

One of the most used methodologies for the synthesis of anisotropic nanoparticles, it is the preparation of seed-mediated growth. This method is based on the formation of spherical nanoparticles through the reduction of the metal with a suitable reducing agent in direct micelles. These “seed” nanoparticles will later be added to a growth solution that contains the same or different ions, along with other additives, such as dopants, ligands, etc. The metal ions of the growth solution are reduced on the surface of the seeds via heterogeneous nucleation during the growth reaction of the particle. Through the variation of the concentration and “seeds” in the growth solution, it is possible to generate a great variety of shapes such as nanorods [72], nanowires [35], nanoplates [19], nanodisks [9] or nanocubes [28]. There are several reports in which this type of methodologies have been used using CTAB surfactant to generate direct micelles [30, 43, 58, 67, 72].

Mandal et al. have been synthesized copper nanoparticles (CuNPs) for the first time using AOT direct micelles. The nanoparticles synthesized were spherical and highly crystalline with a diameter of 5–10 nm. They showed that AOT surfactant had a double role in the synthesis process: reducing and stabilizing. Additionally, these results were compared with the product obtained using AOT/isooctane reverse micelles, concluding that reverse micelles favor the production of smaller nanoparticles (diameter < 4 nm) [37]. Jiang et al. studied the role of temperature in the growth process of silver nanoparticles synthesized through AOT/water direct micelles using three different reducing agents simultaneously: citric acid, ascorbic acid and sodium borohydride. Through this methodology, the authors obtained spherical and triangular AgNPs, whose surface plasmon band was placed in a range of 700–1400 nm, which allow use them in optical applications, such as optical probes, ionic sensors and biochemical sensors [24].

In relation to the synthesis of M-NPs through reverse micelles (RMs), this methodology is based on mixing two identical micellar solutions, each containing one of the reactants (metal precursor and reducing agent), these RMs interact and the metal ions are reduced, then the nucleation and growth occur in a limited space (polar core) [27]. Singha et al. obtained spherical AgNPs from a reverse micelle system (AOT/heptane), using ascorbic acid as a reducing agent. The contribution made by

these authors was to compare the reaction in homogeneous media with the reaction in reverse micelles. The results showed that in homogeneous media, the reaction does not occur at room temperature, whereas when using a reverse micelle media, the reaction proceeds easily [57]. Zhang et al. synthesized nanorods and nanofibers through low intensity ultrasonication using AOT/isooctane reverse micelles system. The results obtained through electron transmission microscopy (TEM) showed that spherical AgNPs were obtained with ultrasonication, and rods and wires shapes were obtained without ultrasonication [70].

Metal nanoparticles have an efficient interaction with light, which results in the release of energy through two main mechanisms: dispersion and absorption. The first mechanism is carried out through the release of photons with the same frequency and the second mechanism is accomplished through conversion of photons into phonons or heat [10]. The relative efficiency of absorption and dispersion of a specific nanoparticle can be quantified through the called photothermal efficiency, which depends strongly on the morphology and size of the nanoparticles [10]. The heating response of nanoparticles has been widely studied, especially the heating response of AuNPs [20, 47, 48, 53]. Despite the advantages of the use of AuNPs, some studies report the use of AgNPs in photothermal therapy against different types of cancer, including ovarian cancer [64]. AgNPs have photothermal and cytotoxic properties, which can be used to generate a synergistic effect [61, 65, 66], which leads to the death of cancer cells. The type of nanostructures that have frequently been used in the field of biomedicine includes nanospheres, nanowires, nanorods, nanoplates and nanocubes [2, 22, 25, 50, 56, 74]. In order to assure the selectivity of NPs in this type of therapies, it is necessary to functionalize NPs with a molecule that gives them the ability to interacting selectively with cancer cells. An example of molecule that has been commonly used for this purpose is folic acid (FA) [6, 33, 68], due to that some cancer cell lines, including those of cervical cancer, present overexpression of folate receptors in comparison with normal cells. This fact, it allows that the NPs can be selectively internalized in the cancer cells through the process of receptor-mediated endocytosis [38].

Here we report the synthesis of functionalized AgNPs with folic acid through two methodologies based on the use of AOT micelles as a reaction media (direct and reverse micelles). The AgNPs obtained were evaluated in HeLa cells (human epitheloid cervix carcinoma), as photothermal agents capable to cause selective death after irradiation with a laser of 808 nm.

2 Experimental section

2.1 Materials

Isooctane (for analysis), silver nitrate (AgNO_3 , for analysis), folic acid ($\text{C}_{19}\text{H}_{19}\text{N}_7\text{O}_6$, for biochemistry), L(+)-ascorbic acid ($\text{C}_6\text{H}_8\text{O}_6$ for analysis) were purchased from Merck, Bis-(2-ethylhexyl)sulfosuccinate sodium salt (AOT, > 96% purity) were purchased from Alfa Aesar, sodium borohydride (NaBH_4 , > 96% purity) were purchased from Panreac, sodium citrate tribasic dihydrate ($\text{HOC}(\text{COONa})(\text{CH}_2\text{COONa})_2 \cdot 2\text{H}_2\text{O}$, > 99.0% purity) and MTT (3-[4,5-dimethylthiazol-2-yl]-2,5-diphenyltetrazolium bromide) were purchased from Sigma Aldrich, citric acid ($\text{C}_6\text{H}_8\text{O}_7$, 99.5% purity) were purchased from JT-Baker. Ultrapure water was obtained from Milli-Q equipment. All the reactants were used without further purification.

HeLa Cells were maintained in EMEM supplemented with 10% of fetal bovine serum (FBS) in a 95% humidified atmosphere and 5% CO_2 at 37 °C. Cells were seeded near confluence a day before incubation with AgNPs.

2.2 Methods

The protocol described by Jiang et al. was used to the synthesis of AgNPs [24], in which 100 mL of a mixture of AgNO_3 and AOT of concentration 2.5×10^{-4} M and 5.0×10^{-4} M were used respectively. Subsequently, different amounts of the aqueous solutions of the reducing agents were added sequentially and under constant stirring: 1.20 mL of citric acid (1.0 M), 0.30 mL of L-ascorbic acid (0.10 M), and 0.02 mL of NaBH_4 (0.002 M). Once the addition of each reducing agent to the reaction mixture was completed, stirring was maintained for ~ 30 s.

In this case a solution of surfactant AOT/isooctane 0.05 M was prepared, an aqueous solution of 0.5 M AgNO_3 was used as metal precursor and aqueous solution of 0.25 M NaBH_4 was used as reducing agent. Then, two identical micellar solutions were mixing by magnetic agitation at room temperature, and each one contains the reactants (AgNO_3 and NaBH_4), these RMs interact and the silver ions are reduced. Nucleation and growth of AgNPs occur in a limited space (polar core) and water to surfactant molar ratio (W_o) used was 5.

The solutions obtained from the synthesis process were deposited in microcentrifuge tubes (2 mL) and centrifuged at 10,619 gravities/min for 20 min. Once the centrifugation process was finished, the supernatant was removed, and the resulting pellet corresponds to the synthesized AgNPs. Subsequently, the pellet obtained

was washed twice with an aqueous solution of 20% ethanol in order to remove the excess surfactant.

With the purpose to eliminate the organic solvent, 1 mL of an aqueous solution of acetone was added to the volume of solution (2 mL) obtained in the above process. After mixing the solutions, two phases were obtained, the organic phase containing the AgNPs and the aqueous phase containing the excess of surfactant. The organic phase is brought to dryness with nitrogen and the resulting solid was washed with a 50% aqueous acetone solution to remove the excess surfactant and centrifuged for 20 min at 10,619 gravities/min. The solid obtained corresponds to the AgNPs.

The AgNPs obtained after the phase transfer and purification process were functionalized with FA, in this sense 2 mL of folic acid aqueous solution (1×10^{-3} M) at pH: 9 (1 M NaOH) was added to the solid obtained in the precipitation and phase transfer process.

These solutions were sonicated for 5 min in order to facilitate the interaction of the AgNPs with the folic acid molecules. Subsequently, they were centrifuged at 10,619 gravities/min for 20 min. Once the centrifugation process was over, the supernatant or excess folic acid was removed.

UV visible spectra were recorded using a spectrophotometer Hewlett Packard-Agilent 8453 with a thermostated sample holder. The path length used in all experiments was 1 cm.

Free FA and AgNP@FA solutions were analyzed by fluorescence spectroscopy with a Perkin Elmer LS-55 spectrofluorimeter. The concentration of the folic acid solution was 5×10^{-5} M. The excitation wavelength was 364 nm. Measurements of Z-potential were performed on a Zetasizer Nano ZS90 equipment, for each solution of AgNPs and AgNP@FA prepared.

For TEM studies, the samples were placed into a formvar-covered copper grid and evaporated slowly. The micrographs were recorded using a Transmission Electron Microscopy (TEM) FEI TECNAI G2 STWIN at 20–200 kV with a camera Gatan ES100W, the images were analyzed and the interplanar crystal spacing was measured using the software Gatan Digital Micrograph, the Miller indices (hkl) were assigned using the JCPDS-ICDD 04-0783 document.

HeLa cells in Eagle's Minimum Essential Medium (EMEM) supplemented with 10% FBS were added in 96 well plate (density of 960.000 cells/well) and incubated for 24 h at 37 °C with 5% CO_2 atmosphere. We studied the effect of AgNP and AgNP@FA concentration over the percentage of viability cell and the effect of irradiation. Cells were treated with different concentrations of AgNPs and AgNPs@FA (20, 100 and 200 μM of Ag) prepared in EMEM medium. Nanoparticles were not added in the case of the control cells.

2 and 4 h of treatment were evaluated in order to the nanoparticles internalization. In the case of the assays without irradiation, once the treatment time was finished, the medium was discarded, and replaced by 200 μL of MTT solution (500 $\mu\text{g}/\text{mL}$ in HBSS solution). The assays were maintaining in incubation for 3 h at 37 $^{\circ}\text{C}$, and subsequently, the MTT solution was discarded and 200 μL of DMSO were added, in order to solubilize the crystals formed. Finally, the plate was read at 570 nm on a Multiskan™ GO microplate reader [44]. The result obtained from reading the plates corresponds to the absorbance values of both the controls and each of the treatment wells. These absorbance values allow calculating cell viability.

In the case of the irradiation assays after the treatment time, the cell medium was removed, and replaced by 200 μL of fresh EMEM, in order to rule out the AgNPs that were not internalized. Finally, the cells were irradiated for 5 min in each well using a diode laser (ThorLabs Newton USA) of 800 nm with 800 mW and the distance between the diode laser and samples was 5 cm.

Once the irradiation process was completed, EMEM medium was removed and the MTT reagent was added. The subsequent steps are the same as those mentioned in the case of assays without irradiation.

Data were presented as means \pm standard error (SE) from at least two independent experiments and compared by analysis of variance one way (ANOVA) followed by multiple comparison analysis averages, Tukey. Differences at $p < 0.05$ were considered statistically significant.

3 Results and discussion

3.1 Determination of critical micelle concentration (CMC)

In each of the micellar systems used as reaction media, the effective formation of the molecular aggregates was ensured through the determination of critical micelle concentration (CMC). For the AOT/water system, there is an only report about the CMC in an aqueous binary system [37]. Taking into account this limitation, in this work, the CMC of the AOT/water system was determined by means of a spectrophotometric method, where the changes in the maximum absorption of the dye methylthionine chloride (methylene blue) were evaluated. Methylene blue exists in the cationic form at neutral pH. The surface of AOT direct micelles being negatively charged, the cationic form of dye will be attracted towards the micellar Stern layer due to electrostatic attraction. The concentration of dye was 1.6×10^{-4} M and surfactant concentrations from 5×10^{-5} to 1×10^{-3} M. Graphing the values λ of the maximum absorption of the dye against the logarithm of the

Table 1 Comparison of the concentrations used in the synthesis processes with the value of the CMC

Micellar system	Concentrations in the synthesis process (moles/L)	CMC (moles/L)
AOT/water	5.0×10^{-4}	4×10^{-4}
AOT/isooctane	5.0×10^{-2}	1.7×10^{-3}

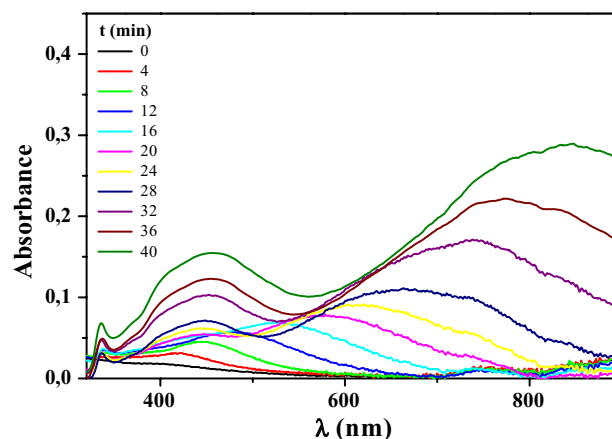


Fig. 1 Absorption spectra of AgNPs formation in AOT/water direct micelles at $[\text{AgNO}_3] = 2.5 \times 10^{-4}$ M, $[\text{AOT}] = 5.0 \times 10^{-4}$ M, $[\text{citric acid}] = 1.0$ M, $[\text{L-ascorbic acid}] = 0.10$ M, $[\text{NaBH}_4] = 0.002$ M and temperature: 23 $^{\circ}\text{C}$

surfactant concentration and using a sigmoidal adjustment, the inflection point was determined, which corresponds to the CMC value of the surfactant in the system. The results obtained from this determination can be seen in Supplementary information (Figure S1).

The value of the CMC for the AOT/water system obtained was 4×10^{-4} M. Table 1 shows the CMC values for each of the systems evaluated together with the concentrations of surfactant that were used in the processes of synthesis. When comparing each of the concentration values in the synthesis process with the values corresponding to the CMC, it is observed that all concentration values used in the synthesis processes are above the CMC.

3.2 Characterization of AgNPs obtained through direct micelle (AOT/water)

The AgNPs obtained through the AOT/water system were characterized by means of UV–Vis spectroscopy. Figure 1 show the kinetic formation of the localized surface plasmon resonance (LSPR) for AgNPs synthesized.

The absorption spectra indicated at 4 min of reaction an initial band located at $\lambda_{\text{max}} = 420$ nm, this band shifts to longer wavelengths and increases its intensity, while around 20 min a new band appeared at $\lambda_{\text{max}} = 335$ nm.

The stability of the reaction took place at 36 min, when a characteristic LSPR with two maxima absorption bands at $\lambda_{\max} = 450$ nm and $\lambda_{\max} = 826$ nm remains constant through the time, these bands correspond to the contributions of the collective oscillation of the electrons of the conduction band of the NPs along the different axes of the nanoparticles [40] which gives rise to the formation of NPs with different morphologies such as spheres, ellipsoidal, triangles and forms not defined (pseudo geometries).

Taking into account the results obtained from the TEM micrograph (Fig. 2c), the histogram presented in Fig. 2b was constructed, as is shown the average diameter of the particles obtained was 21.5 ± 5 nm, and the obtained shapes (triangles, prisms, spheres, and other undefined shapes) (see Fig. 2c) are in concordance to the absorption spectra obtained in Fig. 2a.

With respect to the coexistence of different types of structures, in the study conducted by Jiang et al., they found that this coexistence can be caused by the type of

crystal structure that the AgNPs present, which is a cubic structure centered on the faces (FCC) [23]. The presence of this type of structure (FCC) in the synthesized AgNPs was verified by high resolution micrographs obtained through TEM. Interplanar crystalline spacing was measured using the Gatan Digital Micrograph software, and this was correlated with the respective Miller indexes using document JCPDS-ICDD 04-0783. The measurements of these interplanar distances allowed to identify a plane Ag (200), which is related to the formation of structures of type FCC (Fig. 2d).

In order to determine the surface charge and the stability of the AgNPs, Zeta potential measurements were made. The obtained value was -40.4 ± 7.74 , which correspond to stable particles in aqueous solution (values more positive than $+30$ mV and more negative than -30). Additionally, it is important to mention the obtained value can be associated with the charge that it gives the residual AOT molecules on the surface of the nanoparticle.

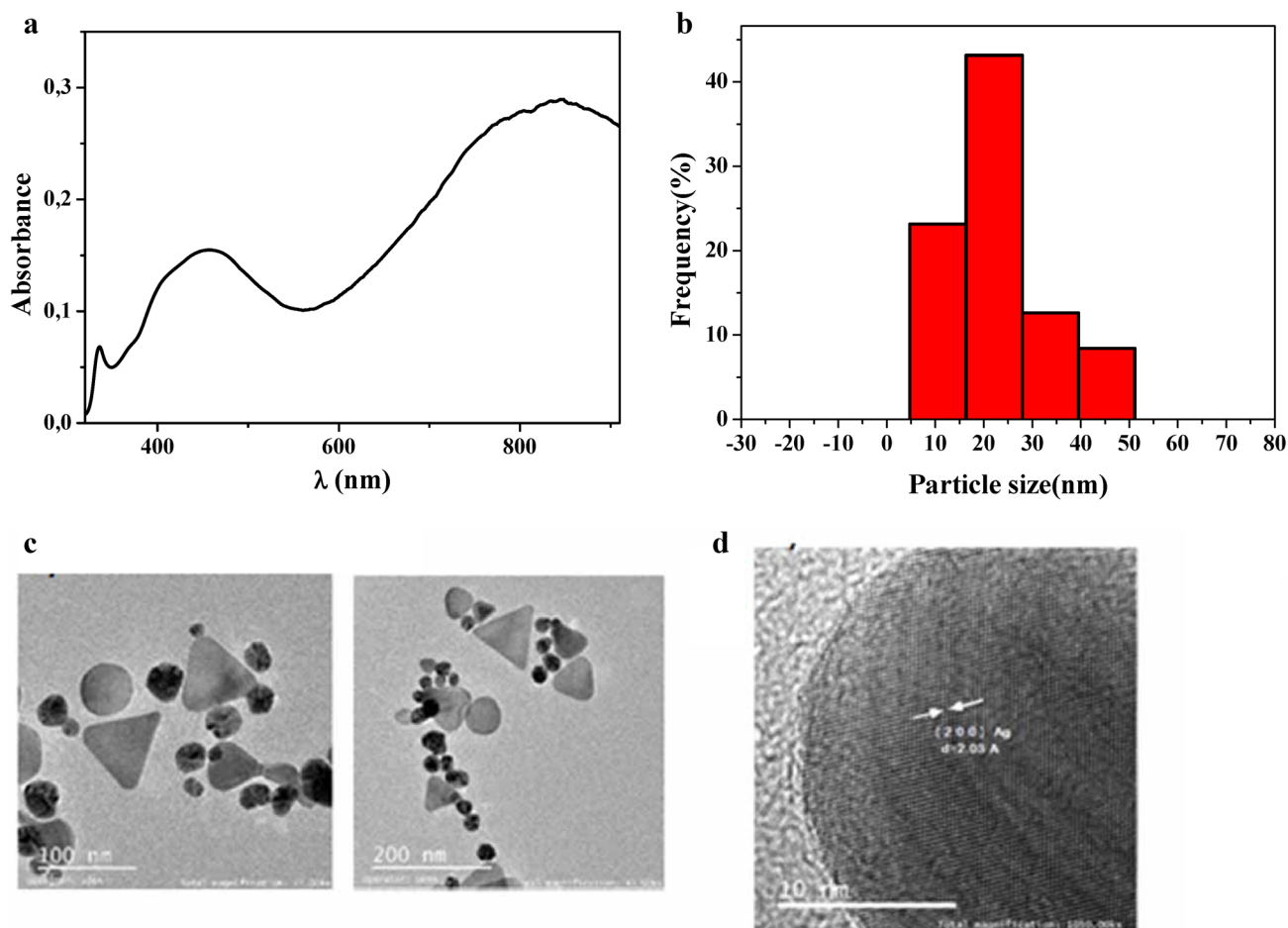


Fig. 2 **a** UV-Vis spectrum of the AgNPs obtained in the AOT/water at $[AgNO_3] = 2.5 \times 10^{-4}$ M, $[AOT] = 5.0 \times 10^{-4}$ M, $[citric\ acid] = 1.0$ M, $[L\text{-ascorbic\ acid}] = 0.10$ M, $NaBH_4 = 0.002$ M and temperature: 23 °C.

b Histogram of particle size distribution by number at the end of the reaction. **c** HR-TEM micrographs. **d** Crystallographic planes

3.3 Characterization of AgNPs obtained through reverse micelle (AOT/isooctane)

AgNPs obtained through the AOT/isooctane system were analyzed through UV–Vis spectroscopy. UV–Vis spectra were taken every 10 s for 2 min. The results obtained are shown in Fig. 3.

Figure 3 shows broad band with a $\lambda_{\max} = 417$ generated when the corresponding volume of AgNO_3 (9 μL) is added to the micellar solution and it becomes a light-yellow coloration through of time. The formation of this band may be associated with the initial reduction of some silver ions in the aqueous core of the micelles due to the effect of the AOT surfactant molecules, thus giving rise to the formation of a small number of seeds. Once the reduction process is started using the reducing agent (NaBH_4), the initial absorption band increases its absorbance and moves smoothly towards longer wavelengths. The stability of this absorption band took place after 2 min of reaction with a λ_{\max} at 427 nm.

The results of the characterization of AgNPs synthesized using the AOT/isooctane reverse micellar system are shown in Fig. 4.

In Fig. 4a the UV–Vis spectrum is shown with a wide band at λ_{\max} around 450 nm. Taking into account the histogram presented in Fig. 4b, it was determined that the average diameter of the particles obtained was 12.61 ± 6 nm, and the shapes of the particles obtained were mostly spheres, together with some anisotropic forms (Fig. 4c). Interplanar crystalline spacing was measured following the same methodology that was used for the previous system. The interplanar distance measurements allowed identifying the Ag (111) and Ag (200) planes, which are related to the formation of structures of type FCC (Fig. 4d).

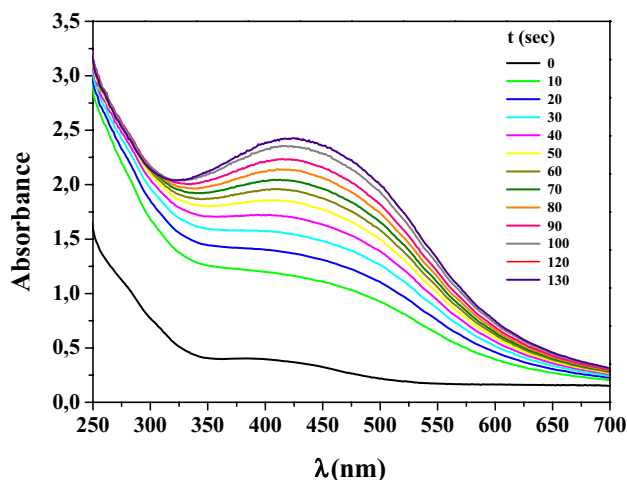


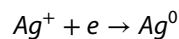
Fig. 3 Absorption spectra of AgNPs formation in AOT/isooctane reverse micelles at $W_0 = 5$, $[\text{AgNO}_3] = 0.5$ M, $[\text{NaBH}_4] = 0.25$ M

Regarding the Zeta potential values, the value obtained for the AgNPs synthesized through RMs were -45.8 ± 5.94 nm. This charge is associated with the charge provided by the residual AOT molecules on the surface of the nanoparticles. Additionally, the value obtained was within the range in which the AgNPs are considered to be stable.

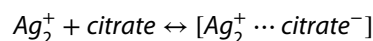
According to the results observed in both systems, the reaction media has an important influence on the nucleation and growth mechanism of AgNPs. The anisotropic structures obtained using direct micelles (DMs) (AOT/water) are attributed to the synergistic effect of reduction using three different types of reducing agents: citric acid, ascorbic acid and NaBH_4 . The co-reduction approach gave a better balance between nucleation and growth of AgNPs, and therefore size and shape controlled silver nanoparticles could be achieved [1].

Among the reducing agents used in the synthesis process, the reducing agent with the lowest reduction potential is citric acid, thus to improve its reduction potential requires high temperature conditions. Jiang et al. showed that the rate of reduction of citric acid is significantly reduced in the presence of the AOT surfactant, due to the formation of the Ag_2 (AOT) and $[\text{Ag}(\text{Cit})_2 \text{AOT}]$ complexes. Additionally, the authors showed the influence of the citric acid molar ratio: silver nitrate ($[\text{Cit}]/[\text{Ag}^+]$). Taking into account the molar ratios used are greater than 40, the reaction becomes slower and therefore takes longer to reach stability. This behavior can be associated to the high concentrations of citrate ions, which give rise to the formation of complexes $[\text{Ag}_2^+ \cdots \text{citrate}^-]$ besides the Ag_2 (AOT), causing a decrease in the rate of the precursor reduction. The formation of these complexes supports the fact that the synthesis process has taken place slowly and the stability of the reaction is only reached until 35 min.

Due to the reduction potential of citric acid is low, the reducing agents that made possible the initial reduction of the Ag^+ ions were ascorbic acid and NaBH_4 . These reducing agents would result in the formation of Ag_2^+ dimers in aqueous solution at the initial stage, as observed in the reactions below:



The dimers formed in the previous step, interact with the citrate ions leading to the formation of complexes $[\text{Ag}_2^+ \cdots \text{citrate}^-]$, which have an influence on the formation and growth rate of AgNPs.



Sodium borohydride (NaBH_4) is considered a strong reducing agent, which in the absence of other reducing

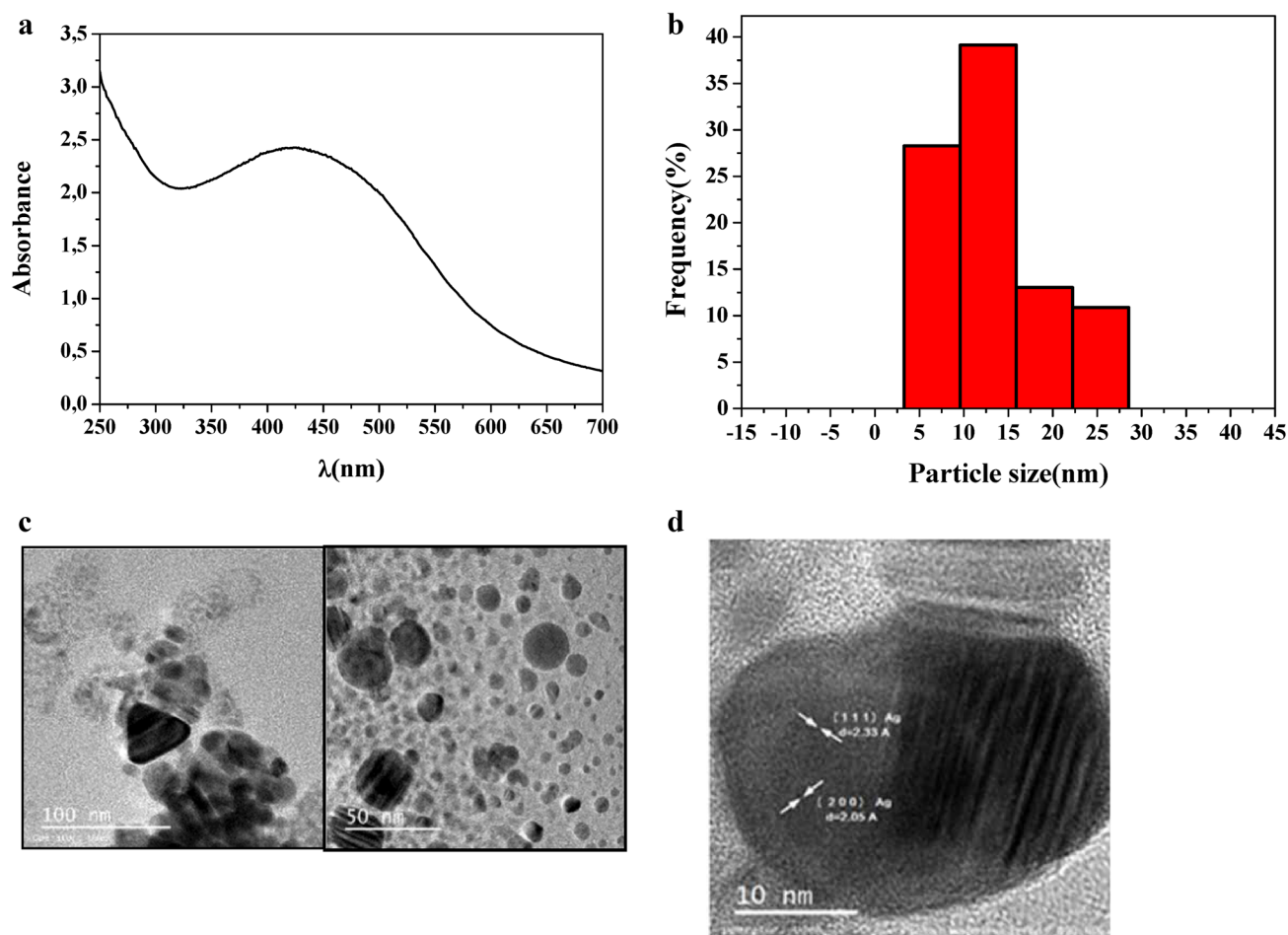


Fig. 4 **a** UV-Vis spectrum of the AgNPs obtained in the AOT/isooctane system at $W_0=5$, $[\text{AgNO}_3]=0.5$ M, $[\text{NaBH}_4]=0.25$ M. **b** Histogram of particle size distribution by number at the end of the reaction. **c** HR-TEM micrographs. **d** Crystallographic planes

agents can lead to the formation of nearly spherical silver particles (~ 5 nm). In order to obtain anisotropic forms using this reducing agent, it is necessary to previously add other weak reducing agents, which will lead to the formation of complexes (i.e., $[\text{Ag}(\text{Cit})_2 \text{AOT}]$), which control the rate of the reaction. Additionally, it is important taking account that in the synthesis process, a low molar ratio of $([\text{BH}_4^-]/[\text{Ag}^+])$ was used because the reduction potential of this reducing agent is high, and to achieve the formation of nanostructures such as nanotriangles, a slow and controlled reaction is required [23].

In addition to the formation of dimers Ag^+ , Jiang et al. reported that under the conditions evaluated also trimeric clusters Ag_3^+ are generated, which can be used as nuclei for the addition of newly formed silver atoms and, finally give place to the formation of silver nanotriangles.

Additionally, it is known that the presence of the AOT surfactant, besides playing an important role in the stability of the AgNPs, also influences the growth processes of these in the presence of silver ions forming complexes

such as Ag_2 (AOT), which affect the reaction rate of the reducing agents, as well as the shape and final size of the particles obtained [23].

In the case of RMs, we used only one reducing agent, because in this systems the reaction is carried out in a confined environment (nanoreactor) where the properties of the aqueous medium are different from those of bulk water [41]. This confined environment allows controlling the shape and size [62]. In the case of this work, we used AOT, which is solubilized in isooctane and carry out the formation of spherical micelles [16] within which generates the reaction. The majority of the authors have reported through these systems (AOT reverse micelles) the obtaining of spherical nanoparticles and sizes between 5 and 10 nm [18, 37, 57, 71]. The influence of the solvent in obtaining these spherical and small nanoparticles, it is important since it has been observed that when using long and linear chain solvents, these affect the micellar interface rigidity, allowing the interface to have a lower rigidity, which gives rise to an increase of intermicellar

exchange rate [5], and in this way, it favors that the reaction between the precursors is quickly. The use of this type of conditions does not favor the obtaining of anisotropic nanoparticles, since the reaction occurs quickly, avoiding the generation of secondary growth processes. In this work, the molar ratio of the precursors was different from the molar ratio that they used and other authors. The molar ratio ($[\text{BH}_4]/[\text{Ag}^+]$) used, less than 1, implies that the metallic precursor (AgNO_3) was in excess which decreases the reaction rate, which allows to modifying the processes of nucleation and growth, that leads to the generation of some anisotropic silver nanoparticles.

3.4 Silver nanoparticles functionalized with folic acid

The AgNPs obtained in both reaction media (direct and reverse micelles) were functionalized with folic acid and characterized by UV–Vis and fluorescence emission spectroscopy. Additionally, Zeta potential measurements were made in order to determine the surface charge and the stability of the AgNPs after functionalization.

The characteristic UV–Vis spectrum of basic form of FA is shown in Figs. 5 and 6. The band around 365 nm is assigned to the $\pi\text{-}\pi^*$ transition localized on the pterin ring of FA [32]. The other bands at 255 and 280 nm are also from $\pi\text{-}\pi^*$ transitions of the pterin [32]. When this molecule interacts with the AgNPs, the band at 255 nm disappear due to this band only appears in the basic form of FA, due to deprotonation of the amine group of the pterin in

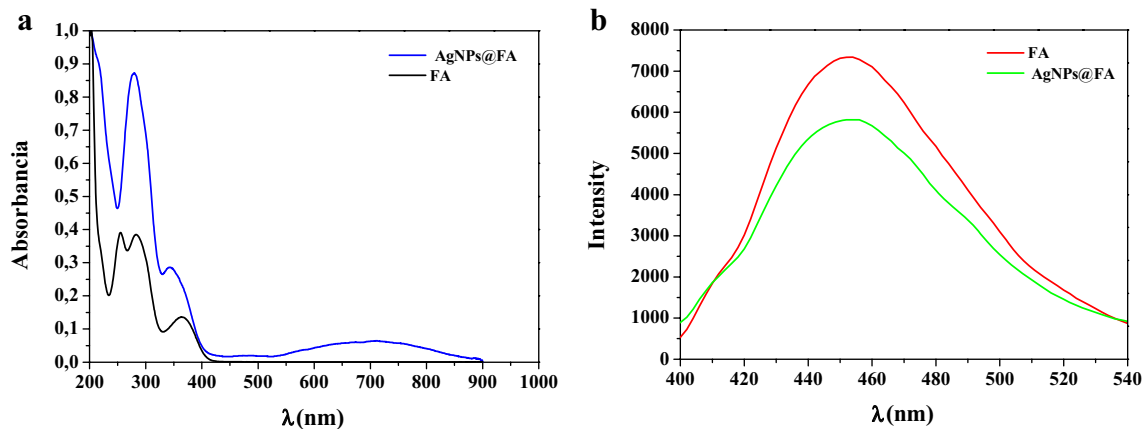


Fig. 5 **a** UV–Vis spectrum and **b** fluorescence emission spectra of FA and the AgNPs@FA obtained by the micellar system AOT/water at [Folic acid] = 5×10^{-5} M, [Ag] = ~ 200 μM , and excitation wavelength used was 364 nm

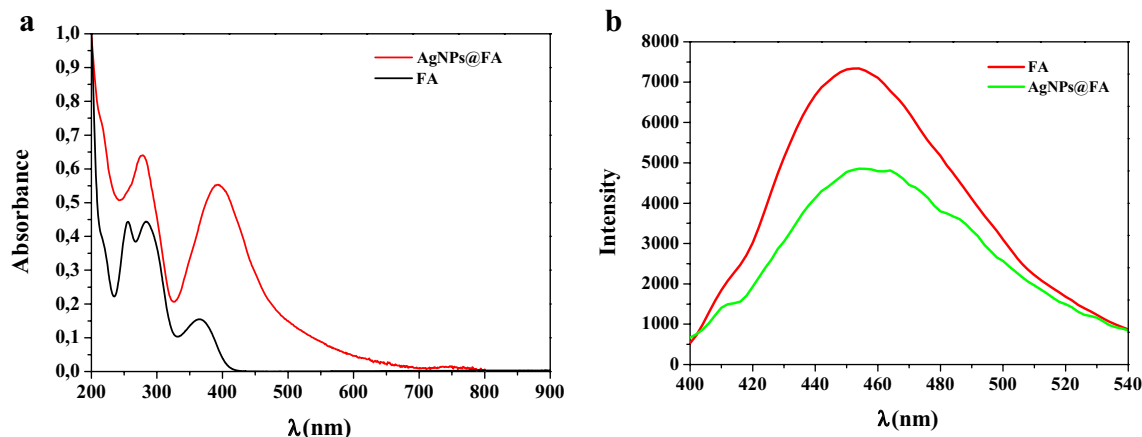


Fig. 6 **a** UV–Vis spectrum and **b** fluorescence emission spectra of FA and the AgNPs@FA obtained by the micellar system AOT/isooctane at [Folic acid] = 5×10^{-5} M, [Ag] = ~ 200 μM , and excitation wavelength used was 364 nm

the anionic form of FA [32]. This modification of the UV–Vis band of FA when it goes from its basic to acid form, it was also evidenced in the study carried out by Li et al. which they carried out pH-dependent, ultrafast time-resolved infrared spectroscopy measurements to understand the excited state electron transfer (ET) reactions of FA in its cationic and anionic forms.

In addition to the UV–Vis spectroscopy analysis, fluorescence emission spectroscopy was performed, the results allow to verify the interaction between NPs and folic acid, through the effect of enhancement or quenching the intensity of the fluorescence of the fluorophore to be bound to the NPs.

Figures 5b and 6b show the fluorescence emission spectra of the AgNPs@FA obtained through micellar system AOT/water, AOT/isooctane and free FA. Quenching of fluorescence of FA in interaction with AgNPs in the two systems is observed. In this sense, it is known the fluorescence of fluorophores could be increased or decreased due to the presence of metallic NPs. This fluorescence behavior is influenced by factors such as the size and shape of the NP, the orientation of the fluorophore, dipole moments relative to the NPs, the rate of radiative decay and quantum yield of the fluorophore [29]. Lakowicz et al. reported that at very short distances (< 5 nm) between the surface of the AgNP and the fluorophore generate a decrease in fluorescence [29].

Among the studies that support this “quenching” effect, Zhao et al. showed a decrease in the fluorescence of 7-methoxy-8-(3-methyl-2-butenyl)-benzopyran-2-one, a coumarin which acts as a blocker of the calcium channels in plants. They determined this decrease in fluorescence occurs and the non-radiating velocity of the fluorophore [73]. Another previous work that is consistent with the quenching effect was carried out by Pramanik et al. They showed that the formation of the stabilizing AOT monolayer does not prevent the close interaction of AgNPs with Safranin molecules (dye) and then showed a decrease in the fluorescence of the dye [51].

Regarding the zeta potential values obtained for AgNPs@FA synthesized through direct and reverse micelles were -34.7 ± 7.03 and -36.3 ± 4.04 respectively. The difference between the values obtained is associated with the exchange of ligands that occurs when functionalizing the AgNPs with folic acid. Additionally, the AgNPs in this range of values observed are considered to be stable [49]. The negative charge on the surface of the nanoparticles could be associated with the presence of the deprotonated carboxyl groups of folic acid [31, 59]. This is in accordance with the study carried out by Su et al., which observed that these groups stabilized the nanoparticles through electrostatic repulsion [59]. It has been shown that the interaction of folic acid with the AgNPs

occurs through the amino group of the pterinic ring of folic acid [7, 8, 31, 59]. Besides, Castillo et al. using the density functional theory to show that the Ag-FA interaction occurs mainly through the nitrogen of the pteridine ring. Additionally, the interactions of folic acid (FA) by surface-enhanced Raman scattering (SERS) was studied [8].

3.5 Biological Assays with HeLa cells

The cytotoxicity of the AgNPs and AgNPs@AF obtained by the micellar system AOT/water and AOT/isooctane were evaluated in the absence of irradiation (Fig. 7). The effect of irradiation on HeLa cells was evaluated using a laser

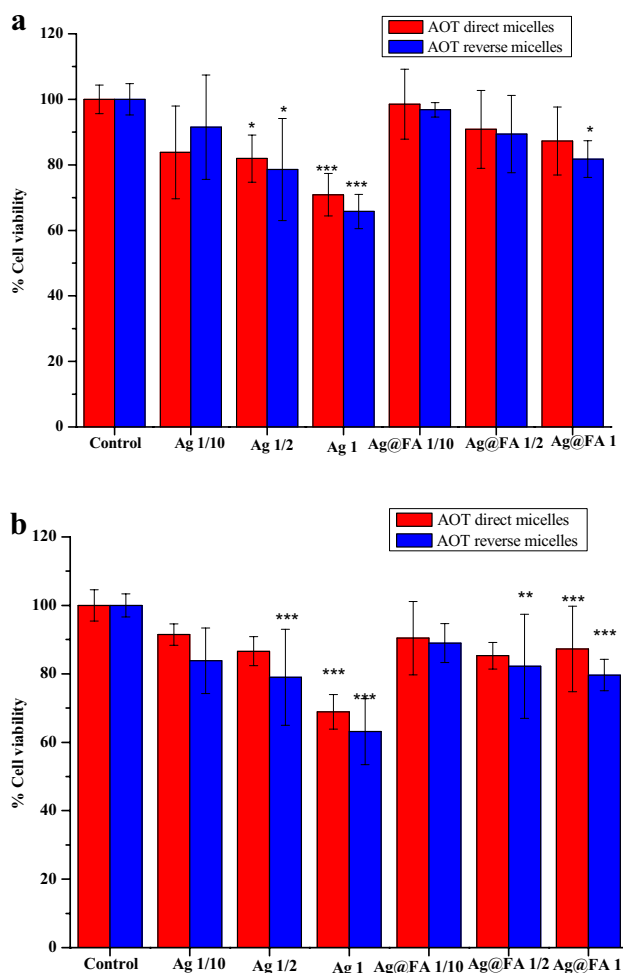


Fig. 7 Cytotoxicity without irradiation of the non-functionalized AgNPs (Ag) and functionalized AgNPs (Ag@FA) synthesized through AOT direct and reverse micelles. The treatment times were **a** 2 h, **b** 4 h. The Ag concentrations evaluated were 200 μ M for Ag 1 and Ag@FA 1, 100 μ M for Ag 1/2 and Ag@FA 1/2 and 20 μ M for Ag 1/10 and Ag@FA 1/10, the control corresponding to HeLa cells not treated. The treatment times were 2 and 4 h, *, **, *** Differences statistically significant with respect to the control, $p < 0.05$, $p < 0.01$, and $p < 0.001$, respectively. Irradiation time per well 5 min

of 808 nm and power of 800 mW (Fig. 8). Additionally, in order to evaluate the internalization by folate receptors two different times of treatment were used (2 and 4 h) (Figs. 7, 8).

Figure 7 shows an effect of particle size on the cytotoxicity of the non-functionalized AgNPs. It was observed that when the particle size decreased, the cytotoxicity in HeLa cells was increased. This result agrees with the study carried out by Kim et al. who evidenced that the smallest sized AgNPs (10 nm size) had a greater apoptotic effect against the MC3T3-E1 cells when compared with other sized AgNPs (50 and 100 nm). These differences are associated in part with their cellular uptake processes from the cell membranes [26]. The cytotoxicity of functionalized

nanoparticles (Ag@FA) showed that the percentage of cell viability increased respect to the nanoparticles without functionalization and also no statistically significant differences were reported with respect to control (HeLa cells not treated with AgNPs), see Fig. 7. In this case, the functionalization of AgNPs perhaps contributes to decreasing of the characteristic cytotoxicity of AgNPs. These results are in agreement with those evidenced by Boca-Farcu et al., which evaluated the cytotoxicity of silver nanotriangles functionalized with FA in an ovarian cancer cell line, evidencing a significant decrease in cytotoxicity with respect to AgNPs without functionalization [6].

Additionally, functionalization with folic acid facilitates the internalization of the particles in the HeLa cells, because folate receptors are highly overexpressed in comparison with normal cells [75]. Thus the functionalization of nanoparticles with folic acid is perhaps an advantage to HeLa Cells photothermal treatment.

The irradiation assays are shown in Fig. 8, the control cells were not affected by the irradiation since there is no statistically significant differences were found between the irradiated and non-irradiated control cells. This can be attributed to the fact that the chromophores present in the tissues do not absorb the infrared radiation [22] and showing that the IRC-induced photothermal therapy is an innocuous technique, that does not affect healthy tissues where the nanoparticles are not internalized [22].

Under the irradiation, the percentages of inhibition of cell viability for the AgNPs obtained through direct and reverse micelles systems at a treatment time of 4 h were 47.3 and 21%, respectively. The highest percentage of inhibition (47.3%) of cell viability is observed in the AOT/water system with a treatment time of 4 h (Fig. 8b). This high inhibition percentage can be related to the anisotropic shape of the nanoparticles (triangular prisms, bars, spheres and other undefined forms), since according to work of Boca-Farcu et al. and Mackey et al., who reported that the triangles, nanoprisms and nanobars, have been shown to be better photothermal agents than nanospheres, in the presence of infrared radiation [6, 36]. Boca-Farcu et al. also mentioned a decrease in cell viability of 69% under irradiation with an 808 nm laser, when evaluating the AgNPs@FA in an ovarian cancer cell line. Despite these authors obtained a better percentage, the conditions evaluated were different that used in this work; they evaluated longer treatment time (24 h) and irradiation time was 10 min per well.

Additionally, the highest percentage of inhibition of cell viability observed in the AOT/water system, it could be related with their plasmon band, which is in the near infrared region, and its absorption coincides with the wavelength of the laser used (808 nm). These AgNPs show greater cell death, which is consistent with the

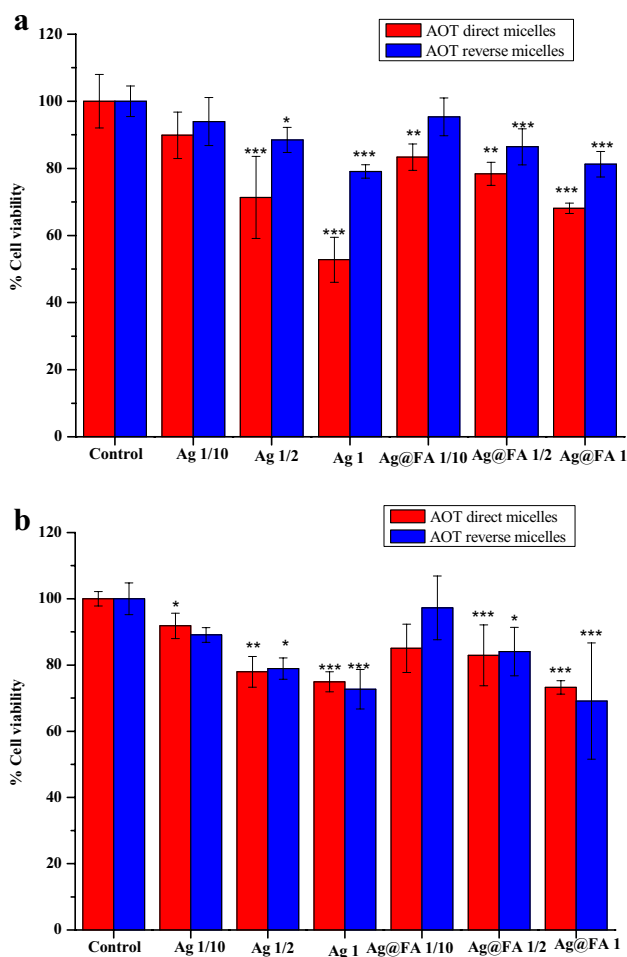


Fig. 8 Cytotoxicity with irradiation (808 nm) of the non-functionalized AgNPs (Ag) and functionalized AgNPs (Ag@FA) synthesized through AOT direct and reverse micelles. The treatment times were **a** 2 h, **b** 4 h. The Ag concentrations evaluated were 200 μ M for Ag 1 and Ag@FA 1, 100 μ M for Ag 1/2 and Ag@FA 1/2 and 20 μ M for Ag 1/10 and Ag@FA 1/10, the control corresponding to HeLa cells not treated. The treatment times were 2 and 4 h, *, **, *** Differences statistically significant with respect to the control, $p < 0.05$, $p < 0.01$, and $p < 0.001$, respectively. Irradiation time per well 5 min

absorption efficiency of irradiation. In addition to the anisotropy of the nanoparticles and the plasmon band, the average size of the AgNPs is also a factor that influences the thermal efficiency of the AgNPs [34, 42]. The average size of the AgNPs obtained with the AOT/isooctane system (10–15 nm) was lower than obtained in the AgNPs with the AOT/water micellar systems (20–50 nm) and it has been indicated according to previous works that the appropriate size to achieve a photothermal effect is around 50 nm, which may explain the difference of the photothermal effect observed.

4 Conclusions

The synthesis of AgNPs using a direct micelles (AOT/water) system permits the formation of anisotropic nanoparticles with 10–50 nm of sizes, while a reverse micelles (AOT/isooctane) system allows nanoparticles spherical with 5–25 nm. Additionally, functionalization with FA allowed decreasing the cytotoxicity without irradiation of the AgNPs obtained by the two micellar systems, allowing to improve its biocompatibility with HeLa cells. Finally, folic acid functionalized AgNPs synthesized by the AOT water system showed to be potentially effective photothermal agents, managing to reduce up to 47.3% of the viability of the HeLa cells, using an 808 nm laser.

Acknowledgements We gratefully acknowledge the financial support for this work by the Universidad Industrial de Santander—UIS (Project 1819 and 2320) and Colciencias (Administrative Department of Science, Technology and Innovation) for the program (Es tiempo de volver) cooperation agreement N° FP44842-507-2014.

Compliance with ethical standards

Conflict of interest The authors declare that they have no conflict of interests.

References

1. Agnihotri S, Mukherji S, Mukherji S (2014) Size-controlled silver nanoparticles synthesized over the range 5–100 nm using the same protocol and their antibacterial efficacy. *RSC Adv* 4(8):3974–3983. <https://doi.org/10.1039/C3RA44507K>
2. An L, Wang Y, Tian Q, Yang S (2017) Small gold nanorods: recent advances in synthesis, biological imaging, and cancer therapy. *Materials* 10(12):1372. <https://doi.org/10.3390/ma10121372>
3. Austin LA, Mackey MA, Dreaden EC, El-Sayed MA (2014) The optical, photothermal, and facile surface chemical properties of gold and silver nanoparticles in biodiagnostics, therapy, and drug delivery. *Arch Toxicol* 88(7):1391–1417. <https://doi.org/10.1007/s00204-014-1245-3>
4. Azizi M, Ghourchian H, Yazdian F, Bagherifam S, Bekhradnia S, Nyström B (2017) Anti-cancerous effect of albumin coated silver nanoparticles on MDA-MB 231 human breast cancer cell line. *Sci Rep* 7(1):5178. <https://doi.org/10.1038/s41598-017-05461-3>
5. Bagwe RP, Khilar KC (2000) Effects of intermicellar exchange rate on the formation of silver nanoparticles in reverse microemulsions of AOT. *Langmuir* 16(3):905–910. <https://doi.org/10.1021/la980248q>
6. Boca-Farcau S, Potara M, Simon T, Juhem A, Baldeck P, Astilean S (2014) Folic acid-conjugated, sers-labeled silver nanotriangles for multimodal detection and targeted photothermal treatment on human ovarian cancer cells. *Mol Pharm* 11(2):391–399. <https://doi.org/10.1021/mp400300m>
7. Castillo JJ, Rindzevicius T, Rozo CE, Boisen A (2015) Adsorption and vibrational study of folic acid on gold nanopillar structures using surface-enhanced Raman scattering spectroscopy. *Nanomater Nanotechnol* 5:29. <https://doi.org/10.5772/61606>
8. Castillo JJ, Rindzevicius T, Wu K, Rozo CE, Schmidt MS, Boisen A (2015) Silver-capped silicon nanopillar platforms for adsorption studies of folic acid using surface enhanced Raman spectroscopy and density functional theory: Ag NP platforms for adsorption studies of FA. *J Raman Spectrosc* 46(11):1087–1094. <https://doi.org/10.1002/jrs.4734>
9. Chen S, Fan Z, Carroll DL (2002) Silver nanodisks: synthesis, characterization, and self-assembly. *J Phys Chem B* 106(42):10777–10781. <https://doi.org/10.1021/jp026376b>
10. de Aberasturi DJ, Serrano-Montes AB, Liz-Marzán LM (2015) Modern applications of plasmonic nanoparticles: from energy to health. *Adv Opt Mater* 3(5):602–617. <https://doi.org/10.1002/adom.201500053>
11. Deraedt C, Salmon L, Gatard S, Ciganda R, Hernandez R, Ruiz J, Astruc D (2014) Sodium borohydride stabilizes very active gold nanoparticle catalysts. *Chem Commun* 50(91):14194–14196. <https://doi.org/10.1039/C4CC05946H>
12. Duque JS, Blandón JS, Riascos H (2017) Localized Plasmon resonance in metal nanoparticles using Mie theory. *J Phys: Conf Ser* 850:012017. <https://doi.org/10.1088/1742-6596/850/1/012017>
13. El-Brolosy TA, Abdallah T, Mohamed MB, Abdallah S, Easawi K, Negm S, Talaat H (2008) Shape and size dependence of the surface plasmon resonance of gold nanoparticles studied by photoacoustic technique. *Eur Phys J Spec Top* 153(1):361–364. <https://doi.org/10.1140/epjst/e2008-00462-0>
14. Fleming DA, Williams ME (2004) Size-controlled synthesis of gold nanoparticles via high-temperature reduction. *Langmuir* 20(8):3021–3023. <https://doi.org/10.1021/la0362829>
15. Ganguli AK, Ganguly A, Vaidya S (2010) Microemulsion-based synthesis of nanocrystalline materials. *Chem Soc Rev* 39(2):474–485. <https://doi.org/10.1039/B814613F>
16. Gochman-Hecht H, Bianco-Peled H (2005) Structure of AOT reverse micelles under shear. *J Colloid Interface Sci* 288(1):230–237. <https://doi.org/10.1016/j.jcis.2005.02.083>
17. Gomaa EZ (2017) Silver nanoparticles as an antimicrobial agent: a case study on *Staphylococcus aureus* and *Escherichia coli* as models for Gram-positive and Gram-negative bacteria. *J Gen Appl Microbiol* 63(1):36–43. <https://doi.org/10.2323/jgam.2016.07.004>
18. Hart AE, Akers DB, Gorosh S, Kitchens CL (2013) Reverse micelle synthesis of silver nanoparticles in gas expanded liquids. *J Supercrit Fluids* 79:236–243. <https://doi.org/10.1016/j.supflu.2013.02.014>
19. Huang W-L, Chen C-H, Huang MH (2007) Investigation of the growth process of gold nanoplates formed by thermal aqueous solution approach and the synthesis of ultra-small gold nanoplates. *J Phys Chem C* 111(6):2533–2538. <https://doi.org/10.1021/jp0672454>
20. Huang X, El-Sayed IH, Qian W, El-Sayed MA (2006) Cancer cell imaging and photothermal therapy in the near-infrared region

- by using gold nanorods. *J Am Chem Soc* 128(6):2115–2120. <https://doi.org/10.1021/ja057254a>
21. Huang X, Jain PK, El-Sayed IH, El-Sayed MA (2008) Plasmonic photothermal therapy (PPTT) using gold nanoparticles. *Lasers Med Sci* 23(3):217–228. <https://doi.org/10.1007/s10103-007-0470-x>
 22. Jaque D, Martínez Maestro L, del Rosal B, Haro-Gonzalez P, Benayas A, Plaza JL, Rodriguez EM, García Solé J (2014) Nanoparticles for photothermal therapies. *Nanoscale* 6(16):9494–9530. <https://doi.org/10.1039/C4NR00708E>
 23. Jiang XC, Chen CY, Chen WM, Yu AB (2010) Role of citric acid in the formation of silver nanoplates through a synergistic reduction approach. *Langmuir* 26(6):4400–4408. <https://doi.org/10.1021/la903470f>
 24. Jiang XC, Chen WM, Chen CY, Xiong SX, Yu AB (2010) Role of temperature in the growth of silver nanoparticles through a synergetic reduction approach. *Nanoscale Res Lett*. <https://doi.org/10.1007/s11671-010-9780-1>
 25. Key J, Dhawan D, Cooper CL, Knapp DW, Kim K, Kwon IC, Choi K, Park K, Decuzzi P, Leary JF (2016) Multicomponent, peptide-targeted glycol chitosan nanoparticles containing ferrimagnetic iron oxide nanocubes for bladder cancer multimodal imaging. *Int J Nanomed* 11:4141–4155. <https://doi.org/10.2147/IJN.S109494>
 26. Kim T-H, Kim M, Park H-S, Shin US, Gong M-S, Kim H-W (2012) Size-dependent cellular toxicity of silver nanoparticles. *J Biomed Mater Res, Part A* 100A(4):1033–1043. <https://doi.org/10.1002/jbm.a.34053>
 27. Krutyakov YA, Kudrinskiy AA, Olenin AY, Lisichkin GV (2008) Synthesis and properties of silver nanoparticles: advances and prospects. *Russ Chem Rev* 77(3):233–257. <https://doi.org/10.1070/RC2008v077n03ABEH003751>
 28. Kundu S, Yi S-I, Ma L, Chen Y, Dai W, Sinyukov AM, Liang H (2017) Morphology dependent catalysis and surface enhanced Raman scattering (SERS) studies using Pd nanostructures in DNA, CTAB and PVA scaffolds. *Dalton Trans* 46(29):9678–9691. <https://doi.org/10.1039/C7DT01474K>
 29. Lakowicz JR (2005) Radiative decay engineering 5: metal-enhanced fluorescence and plasmon emission. *Anal Biochem* 337(2):171–194. <https://doi.org/10.1016/j.ab.2004.11.026>
 30. Lee G (2004) Preparation of silver nanorods through the control of temperature and pH of reaction medium. *Mater Chem Phys* 84(2–3):197–204. <https://doi.org/10.1016/j.matchemphys.2003.11.024>
 31. Li G, Li D, Zhang L, Zhai J, Wang E (2009) One-step synthesis of folic acid protected gold nanoparticles and their receptor-mediated intracellular uptake. *Chem Eur J* 15(38):9868–9873. <https://doi.org/10.1002/chem.200900914>
 32. Li G, Magana D, Dyer RB (2012) Photoinduced electron transfer in folic acid investigated by ultrafast infrared spectroscopy. *J Phys Chem B* 116(10):3467–3475. <https://doi.org/10.1021/jp300392a>
 33. Li H, Cheng Y, Liu Y, Chen B (2016) Fabrication of folic acid-sensitive gold nanoclusters for turn-on fluorescent imaging of overexpression of folate receptor in tumor cells. *Talanta* 158:118–124. <https://doi.org/10.1016/j.talanta.2016.05.038>
 34. Liu X, Shan G, Yu J, Yang W, Ren Z, Wang X, Xie X, Chen HJ, Chen X (2017) Laser heating of metallic nanoparticles for photothermal ablation applications. *AIP Adv* 7(2):025308. <https://doi.org/10.1063/1.4977554>
 35. Liu Y, Hou D, Wang G (2003) Synthesis and characterization of SnS nanowires in cetyltrimethylammoniumbromide (CTAB) aqueous solution. *Chem Phys Lett* 379(1–2):67–73. <https://doi.org/10.1016/j.cplett.2003.08.014>
 36. Mackey MA, Ali MRK, Austin LA, Near RD, El-Sayed MA (2014) The most effective gold nanorod size for plasmonic photothermal therapy: theory and in vitro experiments. *J Phys Chem B* 118(5):1319–1326. <https://doi.org/10.1021/jp409298f>
 37. Mandal S, De S (2016) Copper nanoparticles in AOT “revisited”-direct micelles versus reverse micelles. *Mater Chem Phys* 183:410–421. <https://doi.org/10.1016/j.matchemphys.2016.08.046>
 38. Mehra NK, Mishra V, Jain NK (2013) Receptor-based targeting of therapeutics. *Ther Deliv* 4(3):369–394. <https://doi.org/10.4155/tde.13.6>
 39. Mittal AK, Chisti Y, Banerjee UC (2013) Synthesis of metallic nanoparticles using plant extracts. *Biotechnol Adv* 31(2):346–356. <https://doi.org/10.1016/j.biotechadv.2013.01.003>
 40. Mogensen KB, Kneipp K (2014) Size-dependent shifts of plasmon resonance in silver nanoparticle films using controlled dissolution: monitoring the onset of surface screening effects. *J Phys Chem C* 118(48):28075–28083
 41. Moilanen DE, Fenn EE, Wong D, Fayer MD (2009) Water dynamics in large and small reverse micelles: from two ensembles to collective behavior. *J Chem Phys* 131(1):014704. <https://doi.org/10.1063/1.3159779>
 42. Momen HM (2016) Effects of particle size and laser wavelength on heating of silver nanoparticles under laser irradiation in liquid. *Pramana* 87(2):26. <https://doi.org/10.1007/s12043-016-1233-7>
 43. Morsin M, Salleh MM, Sahdana MZ, Mahmud F (2017) Investigation on the growth process of gold nanoplates formed by seed mediated growth method. *Proc Eng* 184:637–642. <https://doi.org/10.1016/j.proeng.2017.04.130>
 44. Mosmann T (1983) Rapid colorimetric assay for cellular growth and survival: application to proliferation and cytotoxicity assays. *J Immunol Methods* 65(1–2):55–63. [https://doi.org/10.1016/0022-1759\(83\)90303-4](https://doi.org/10.1016/0022-1759(83)90303-4)
 45. MubarakAli D, Thajuddin N, Jeganathan K, Gunasekaran M (2011) Plant extract mediated synthesis of silver and gold nanoparticles and its antibacterial activity against clinically isolated pathogens. *Colloids Surf B* 85(2):360–365. <https://doi.org/10.1016/j.colsurfb.2011.03.009>
 46. Mulfinger L, Solomon SD, Bahadory M, Jeyarajasingam AV, Rutkowsky SA, Boritz C (2007) Synthesis and study of silver nanoparticles. *J Chem Educ* 84(2):322
 47. Nam J, Won N, Jin H, Chung H, Kim S (2009) pH-induced aggregation of gold nanoparticles for photothermal cancer therapy. *J Am Chem Soc* 131(38):13639–13645. <https://doi.org/10.1021/ja902062j>
 48. Neshastehriz A, Tabei M, Maleki S, Eynali S, Shakeri-Zadeh A (2017) Photothermal therapy using folate conjugated gold nanoparticles enhances the effects of 6 MV X-ray on mouth epidermal carcinoma cells. *J Photochem Photobiol, B* 172:52–60. <https://doi.org/10.1016/j.jphotobiol.2017.05.012>
 49. Paszkiewicz M, Gołbiewska A, Rajski Ł, Kowal E, Sajdak A, Zaleska-Medynska A (2016) Synthesis and characterization of monometallic (Ag, Cu) and bimetallic Ag–Cu particles for antibacterial and antifungal applications. *Journal of Nanomater* 2016:1–11. <https://doi.org/10.1155/2016/2187940>
 50. Peng F, Su Y, Ji X, Zhong Y, Wei X, He Y (2014) Doxorubicin-loaded silicon nanowires for the treatment of drug-resistant cancer cells. *Biomaterials* 35(19):5188–5195. <https://doi.org/10.1016/j.biomaterials.2014.03.032>
 51. Pramanik S, Bhattacharya SC, Imae T (2007) Fluorescence quenching of 3,7-diamino-2,8-dimethyl-5-phenyl phenazinium chloride by AgCl and Ag nanoparticles. *J Lumin* 126(1):155–159. <https://doi.org/10.1016/j.jlumin.2006.06.008>
 52. Qasim M, Udumluck N, Chang J, Park H, Kim K (2018) Antimicrobial activity of silver nanoparticles encapsulated in poly-N-isopropylacrylamide-based polymeric nanoparticles. *Int J Nanomed* 13:235–249. <https://doi.org/10.2147/IJN.S153485>

53. Rengan AK, Bukhari AB, Pradhan A, Malhotra R, Banerjee R, Srivastava R, De A (2015) In Vivo analysis of biodegradable liposome gold nanoparticles as efficient agents for photothermal therapy of cancer. *Nano Lett* 15(2):842–848. <https://doi.org/10.1021/nl5045378>
54. Roldán MV, Pellegrini N, de Sanctis O (2013) Electrochemical method for Ag-PEG nanoparticles synthesis. *J Nanopart* 2013:1–7. <https://doi.org/10.1155/2013/524150>
55. Sau TK, Rogach AL (2010) Nonspherical noble metal nanoparticles: colloid-chemical synthesis and morphology control. *Adv Mater* 22(16):1781–1804. <https://doi.org/10.1002/adma.200901271>
56. Shao J, Griffin RJ, Galanzha EI, Kim J-W, Koonce N, Webber J, Mustafa T, Biris AS, Nedosekin DA, Zharov VP (2013) Photothermal nanodrugs: potential of TNF-gold nanospheres for cancer theranostics. *Sci Rep* 3(1):1293. <https://doi.org/10.1038/srep01293>
57. Singha D, Barman N, Sahu K (2014) A facile synthesis of high optical quality silver nanoparticles by ascorbic acid reduction in reverse micelles at room temperature. *J Colloid Interface Sci* 413:37–42. <https://doi.org/10.1016/j.jcis.2013.09.009>
58. Smith DK, Korgel BA (2008) The importance of the ctab surfactant on the colloidal seed-mediated synthesis of gold nanorods. *Langmuir* 24(3):644–649. <https://doi.org/10.1021/la703625a>
59. Su D, Yang X, Xia Q, Zhang Q, Chai F, Wang C, Qu F (2014) Folic acid functionalized silver nanoparticles with sensitivity and selectivity colorimetric and fluorescent detection for Hg²⁺ and efficient catalysis. *Nanotechnology* 25(35):355702. <https://doi.org/10.1088/0957-4484/25/35/355702>
60. Sun K, Qiu J, Liu J, Miao Y (2009) Preparation and characterization of gold nanoparticles using ascorbic acid as reducing agent in reverse micelles. *J Mater Sci* 44(3):754–758. <https://doi.org/10.1007/s10853-008-3162-4>
61. Thompson EA, Graham E, MacNeill CM, Young M, Donati G, Wailes EM, Jones BT, Levi-Polyachenko NH (2014) Differential response of MCF7, MDA-MB-231, and MCF 10A cells to hyperthermia, silver nanoparticles and silver nanoparticle-induced photothermal therapy. *Int J Hyperther* 30(5):312–323. <https://doi.org/10.3109/02656736.2014.936051>
62. Tojo C, González E, Vila-Romeu N (2014) The impact of the confinement of reactants on the metal distribution in bimetallic nanoparticles synthesized in reverse micelles. *Beilstein J Nanotechnol* 5:1966–1979. <https://doi.org/10.3762/bjnano.5.206>
63. Tsai M-F, Chang S-HG, Cheng F-Y, Shanmugam V, Cheng Y-S, Su C-H, Yeh C-S (2013) Au nanorod design as light-absorber in the first and second biological near-infrared windows for in vivo photothermal therapy. *ACS Nano* 7(6):5330–5342. <https://doi.org/10.1021/nn401187c>
64. Van de Broek B, Devoogdt N, D'Hollander A, Gijss H-L, Jans K, Lagae L, Muyldermans S, Maes G, Borghs G (2011) Specific cell targeting with nanobody conjugated branched gold nanoparticles for photothermal therapy. *ACS Nano* 5(6):4319–4328. <https://doi.org/10.1021/nn102336g>
65. Wang R, Chen C, Yang W, Shi S, Wang C, Chen J (2013) Enhancement effect of cytotoxicity response of silver nanoparticles combined with thermotherapy on C6 rat glioma cells. *J Nanosci Nanotechnol* 13(6):3851–3854. <https://doi.org/10.1166/jnn.2013.7156>
66. Wang Z, Chang Z, Lu M, Shao D, Yue J, Yang D, Li M, Dong W (2017) Janus silver/silica nanoplatforms for light-activated liver cancer chemo/photothermal therapy. *ACS Appl Mater Interfaces* 9(36):30306–30317. <https://doi.org/10.1021/acsami.7b06446>
67. Xie X, Gao G, Pan Z, Wang T, Meng X, Cai L (2015) Large-scale synthesis of palladium concave nanocubes with high-index facets for sustainable enhanced catalytic performance. *Sci Rep* 5(1):8515. <https://doi.org/10.1038/srep08515>
68. Xu J, Shen X, Jia L, Xu Z, Zhou T, Li X, Ma T, Li H, Wang Y, Zhu T (2017) Facile synthesis of folic acid-conjugated fluorapatite nanocrystals for targeted cancer cell fluorescence imaging. *Mater Lett* 203:37–41. <https://doi.org/10.1016/j.matlet.2017.05.102>
69. Zaarour M, El Roz M, Dong B, Retoux R, Aad R, Cardin J, Dufour C, Gourbilleau F, Gilson JP, Mintova S (2014) Photochemical preparation of silver nanoparticles supported on zeolite crystals. *Langmuir* 30(21):6250–6256. <https://doi.org/10.1021/la5006743>
70. Zhang J, Han B, Liu M, Liu D, Dong Z, Liu J, Li D, Wang J, Dong B, Zhao H, Rong L (2003) Ultrasonication-induced formation of silver nanofibers in reverse micelles and small-angle X-ray scattering studies. *J Phys Chem B* 107(16):3679–3683. <https://doi.org/10.1021/jp026738f>
71. Zhang W, Qiao X, Chen J, Wang H (2006) Preparation of silver nanoparticles in water-in-oil AOT reverse micelles. *J Colloid Interface Sci* 302(1):370–373. <https://doi.org/10.1016/j.jcis.2006.06.035>
72. Zhang W, Hu G, Zhang W, Qiao X, Wu K, Chen Q, Cai Y (2014) Surfactant-directed synthesis of silver nanorods and characteristic spectral changes occurred by their morphology evolution. *Physica E* 64:211–217. <https://doi.org/10.1016/j.physe.2014.07.029>
73. Zhao H, Song F, Zhang J, Wang F, Liu J, Liu Y (2013) Fluorescence quenching of osthole by silver nanoparticles. *J Opt Soc Am B* 30(9):2387. <https://doi.org/10.1364/JOSAB.30.002387>
74. Zhao Y, Liu W, Tian Y, Yang Z, Wang X, Zhang Y, Tang Y, Zhao S, Wang C, Liu Y, Sun J, Teng Z, Wang S, Lu G (2018) Anti-EGFR peptide-conjugated triangular gold nanoplates for computed tomography/photoacoustic imaging-guided photothermal therapy of non-small cell lung cancer. *ACS Appl Mater Interfaces* 10(20):16992–17003. <https://doi.org/10.1021/acsami.7b19013>
75. Zwicke GL, Ali Mansoori G, Jeffery CJ (2012) Utilizing the folate receptor for active targeting of cancer nanotherapeutics. *Nano Rev* 3(1):18496. <https://doi.org/10.3402/nano.v3i0.18496>

Publisher's Note Springer Nature remains neutral with regard to jurisdictional claims in published maps and institutional affiliations.